Transportation Infrastructure Geotechnology (2023) 10:391–423
https://doi.org/10.1007/s40515-022-00226-6

TECHNICAL PAPER

Liquefaction Susceptibility of Cohesionless Soils Under Monotonic Compression and Cyclic Simple Shear Loading at Drained/Undrained/Partially Drained Modes

Sheetal Gujrati[1] · Majid Hussain[1] · Ajanta Sachan[1]

Accepted: 17 January 2022 / Published online: 29 January 2022

Abstract

Liquefaction susceptibility of cohesionless soils is influenced by various factors such as stress state, loading conditions, and shearing modes, and therefore, the implicit assumption of completely undrained shearing modes could pose damaging consequences. In the current research, the effect of stress state and shearing modes on liquefaction response of cohesionless soils was studied under monotonic compression and cyclic simple shear loading conditions. Undrained, drained, and partially drained shearing modes were applied on three different silty sands collected from three different locations of earthquake-prone region of Kutch. The partially drained shearing mode was applied at different effective stress ratios (ESRs) to simulate different stress states. All three silty sands exhibited undrained instability at large ESR values. The effect of cyclic stress ratio (CSR) on liquefaction response of cohesionless soils was also evaluated by conducting cyclic simple shear tests. Soil specimens from all the three locations exhibited liquefaction due to the generation of large excess pore water pressure of greater than 95% of the loss in effective stress. The number of cycles required to initiate liquefaction decreased and the rate of development of pore water pressure increased with the increase in the applied CSR under cyclic simple shear loading conditions.

Keywords Instability · Effective stress ratio · Cohesionless soils · Cyclic resistance ratio · Cyclic simple shear

✉ Ajanta Sachan
ajanta@iitgn.ac.in

Sheetal Gujrati
sheetal.gujrati@alumni.iitgn.ac.in

Majid Hussain
majid.hussain@alumni.iitgn.ac.in

[1] IIT Gandhinagar, Palaj, Gandhinagar, Gujarat 382055, India

Notations

A_f	Skempton's pore pressure parameter at failure during shearing stage
B	Skempton's pore pressure parameter
CD	Consolidated drained
CP	Collapse potential
CU	Consolidated undrained
CRR	Cyclic resistance ratio
CSR	Cyclic stress ratio
CSS	Cyclic simple shear
DFE	drained failure envelope
D	Damping ratio
ESP	Effective stress path
ESR	Effective stress ratio
e	Global void ratio
e_o	Initial void ratio
e_s	Intergranular void ratio
e_f	Interfine void ratio
GSD	Grain size distribution
G	Shear modulus
G_0	Shear modulus at the first loading cycle
I_B	Undrained brittleness index
IL	Instability line
L_p	Liquefaction potential
p'	Mean effective confining pressure
q	Deviatoric stress
r_u	Excess pore pressure ratio
q_{max}	Peak of effective stress path
SM	Silty sand
SA	Strain amplitude
Δu	Excess pore water pressure
σ_c	Confining pressure
σ_{ss}	Steady-state strength
σ_{dmax}	Peak deviatoric stress
σ_{vi}	Vertical overburden pressure
ψ	State parameter
η_{IS}	Effective stress ratio of instability line
ε_a	Axial strain
ε_v	Volumetric strain
δ	Cyclic degradation index

1 Introduction

Embankment on saturated loose cohesionless soil is easily liquefied and damaged during earthquake shaking (Park et al. 2000). Liquefaction of natural soil deposits has been a significant cause of the failure of geotechnical structures in the form of

flow slides under monotonic and cyclic loading conditions. Slope failure in highway and railway embankments due to monotonic loading (Park et al. 2000), shear failure due to fluidization of subgrade under undrained cyclic triaxial loading (Indraratna et al. 2020), and liquefaction-induced failure due to earthquake shaking (Zhong-Ming et al. 2020; Ioanna et al. 2018; Pham and Dias 2019) were reported in the literature. Major loss in shear strength within the soil mass due to the generation of excess pore water pressure (Δu) under undrained shearing conditions was referred to as liquefaction (Hussain and Sachan 2019a). It could be manifested as the extreme consequences of solid–fluid instability in granular materials (Lade and Liggio 2014). The various interpretation methods for liquefaction under monotonic loading, including a steady-state approach and collapse line approach were used to analyze the laboratory test results on the soil mixtures by previous researchers (Wei and Yang 2014; Belkhatir et al. 2011; Amini and Qi 2000). Experimental investigations, including triaxial tests (Thevanayagam 1998; Monkul and Yamamuro 2011) and plane strain tests (Chu and Wanatowski 2008), were performed to investigate the onset of instability in granular materials under different boundary and loading conditions. Over the past two decades, persistent efforts have been made to understand the static liquefaction behavior of silty sands. Most of these studies were based on the use of sand-fines mixtures created using standard river sands such as Nevada sand, Hostan sand, and Ottawa sand with non-plastic and plastic fines such as Sil-co-Sil fines, Potsdam fines, and Kaolin clay (Yamamuro and Lade 1997; Bouferra and Shahrour 2004; Monkul and Yamamuro 2010). The geotechnical properties of natural soil deposits are used for the design and construction of civil engineering structures. The coupled influence of fines content, the plasticity of fines, and the gradation of soil pose a difficulty in understanding the behavior of natural soil deposits. The liquefaction behavior of naturally occurring soil deposits under monotonic and dynamic loading conditions is required for extensive research. In static liquefaction and instability problems, the implicit assumption of completely undrained conditions is assumed before the initiation of instability, followed by liquefaction. However, in several instances, a globally drained soil mass experiences a local loss in effective stress due to smaller local undrained soil mass. This condition refers to different initial stress states other than fully undrained conditions. Different stress path loading such as effective stress increments under various degrees of drainage (Vaid and Eliadorani 1998), shearing at different stress ratios on drained stress path (Chu and Leong 2002), constant shear drained tests (Daouadji et al. 2010), and partially drained conditions through imposed volume changes (Lade and Liggio 2014). Further studies are required to understand the effect of stress state on naturally occurring silty sands under different boundary conditions. Studies were conducted on the cyclic liquefaction behavior of sands and sand-fines mixtures using cyclic triaxial tests (Erten and Maher 1995; Liu 2020). Also, the cyclic simple shear (CSS) apparatus is designed to replicate the earthquake loading conditions more efficiently by applying shear stresses and shear strains directly. In the present study, the influence of stress state on three different naturally occurring silty sands under mix drained conditions under static loading conditions and the liquefaction susceptibility under CSS conditions was explored. The triaxial tests were performed to study the static liquefaction susceptibility of silty sands. The stability of soil under imposed stress

changes was investigated by conducting the mix drained conditions at different effective stress ratios (ESR = q/p').

2 Material Properties and Experimental Program

The soil samples were collected from three different locations of Kutch region, which experienced liquefaction in previous earthquakes. These soil samples were collected from the depth of 1.5 m from the three locations, i.e., site 1: Fatehgarh; site 2: Chang; and site 3: Suvai. The basic geotechnical properties of these three soil sites are presented in Table 1. The initial material state was represented by the initial void ratio (in situ void ratio, e_0) and the fines content (FC) of the prepared soil specimen.

The experimental program consisted of three series of isotropically consolidated triaxial compression tests and cyclic simple shear tests under different boundary conditions. The first and second series of triaxial tests comprised of consolidated undrained (CU) and consolidated drained (CD) triaxial compression tests respectively on the reconstituted samples collected from soil sites 1, 2, and 3. Another series of triaxial tests to investigate the effect of stress ratio on liquefaction behavior was conducted by performing drained tests until a pre-calculated effective stress ratio (ESR) value was obtained, and then shearing was continued under imposed undrained conditions. All three series of triaxial tests were performed at an initial confining pressure of 100 kPa, and shearing was carried out at a deformation rate of 0.1 mm/min. The soil specimens (triaxial tests: 50 mm diameter and 100 mm height, and CSS tests: 70 mm diameter and 20 mm height) were prepared at an in situ dry density and moisture content using the moist tamping method (ASTM D4767–04 2018). Oven-dried soil equivalent to the in situ dry density of the specimens for a volume of 196.34 cm^3 for triaxial tests and 76.96 cm^3 for CSS tests was weighed and thoroughly mixed with the required amount of water corresponding to the in situ water content.

Table 1 Basic geotechnical properties of soils from sites 1, 2, and 3

Geotechnical property	Site 1	Site 2	Site 3
Specific gravity	2.68	2.72	2.72
Gravel (%)	1	8	4
Sand (%)	54	67	80
Silt (%)	34	23	13
Clay (%)	11	2	3
Soil classification	SM	SM	SM
Optimum moisture content (OMC), (%)	9.8	10.8	8.4
Maximum dry density (MDD), (g/cm^3)	2.0	1.97	1.9
Angle of internal friction (ϕ), degrees	35	32	31
Visual appearance	Brown	Dark brown	Gray

SM silty sand

The soil–water mixture was kept for curing for 2 h to ensure equilibration of water content. The mixture of dry soil and water was moist tamped in three layers of equal height having the same amount of soil. For each layer, equal amount of the mixture was transferred to the assembled split mold and tamped by using a mild steel hammer and a wooden block. The compacted specimens were leveled and weighed to confirm the attainment of the required density. The number of layers was kept equal to three for all the specimens. The initial void ratio (e_0) and the FC of soil specimens from sites 1, 2, and 3 are presented in Tables 1 and 2. The saturation of the specimens in all the triaxial tests was ensured by applying enough back pressure to acquire the B value of more than 0.95. Stress-controlled cyclic simple shear tests were conducted at different cyclic stress ratios (CSR = 0.05, 0.075, 0.1, 0.15, and 0.2) on soils from sites 1, 2, and 3 at a vertical pressure of 100 kPa. Figure 1 shows the schematic to explain loading and boundary conditions of the specimen during stress-controlled CSS testing. (Hussain and Sachan 2019b) provided detailed explanation about stress-controlled CSS testing, and the same procedure was followed in the current study. The frequency of 1 Hz was selected to simulate the earthquake loading conditions (Ishihara 1996). Under the applied loading, the strain evolved and accumulated with the number of cycles leading to cyclic degradation, which in extreme cases resulted into liquefaction.

3 Results and Discussion

Liquefaction response of cohesionless soils under monotonic compression (one-directional loading) at three different shearing modes (drained, undrained, partially drained) was evaluated by conducting triaxial tests at three different effective stress ratios. Liquefaction under field conditions is better simulated by K_0 consolidation; therefore, liquefaction susceptibility and dynamic behavior of cohesionless soils were evaluated by conducting a series of cyclic simple shear tests (two-directional loading) under undrained shearing mode. Monotonic compression loading is applied on the specimen in one direction until the specimen fails. However, cyclic simple shear loading is applied in two opposite directions (back and forth) until the specimen fails.

Table 2 Undrained shear response and liquefaction parameters of soils from sites 1, 2, and 3

Specimen	q_{max} (kPa)	u_{peak} (kPa)	σ_{ss} (kPa)	e_o	I_B	CP	L_p
SU1	49	50	12	0.726	0.77	0.90	15.70
SU2	38	36	9	0.735	0.77	0.83	16.14
SU3	35	47	1	0.990	0.97	0.90	19.00

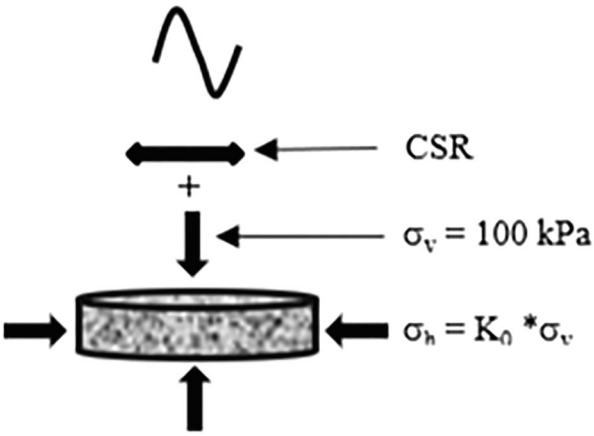

Fig. 1 Loading and boundary conditions in stress-controlled CSS testing

3.1 Liquefaction Susceptibility Under Monotonic Compression

Figure 2 shows the effective stress paths (ESP) of soils from sites 1, 2, and 3 plotted in q-p' stress space under undrained conditions. The specimens for this series of triaxial tests from sites 1, 2, and 3 were tagged as SU1, SU2, and SU3. The peak of

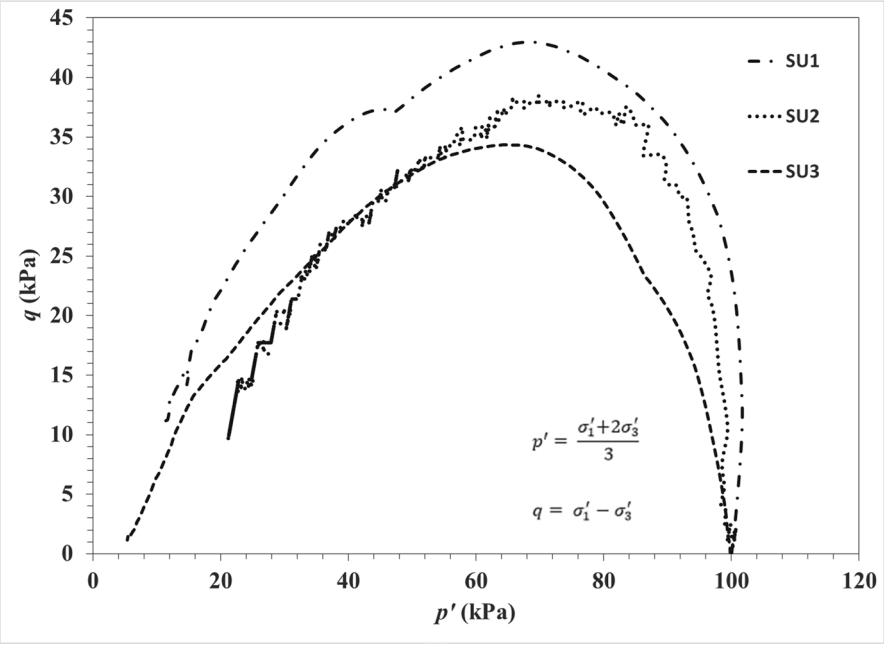

Fig. 2 Effective stress paths in q-p' space of soils from sites 1, 2, and 3 under undrained conditions

ESPs (q_{max}) for all three specimens was obtained to be different (Table 2). SU1 and SU3 exhibited the highest and lowest q_{max} values, respectively. The ESPs ascended to achieve q_{max} and subsequently descended towards the stress origin in all three cases. The generation of Δu led to the reduction in p' which consequently resulted in the loss of shear strength, higher loss for SU3 owing to the higher Δu (95 kPa) developed during undrained shearing. The influence of e_0 on the shear strength of SU1, SU2, and SU3 was reflected through the variation in q_{max}. Although the q_{max} was achieved earlier in SU1 and SU2, ESP of SU3 was found to descend quickly towards the stress origin with continued shear deformation. Generation of large Δu resulted in a loss of p', causing complete static liquefaction of SU3; however, lower Δu in specimens SU2 and SU3 resulted in limited static liquefaction with significant residual strengths. Steady-state strength (σ_{ss}) values were observed to decrease with a decrease in FC (Table 2). Liquefaction susceptibility of soils from sites 1, 2, and 3 was quantified by evaluating liquefaction indices including undrained brittleness index (I_B), collapse potential (CP), and liquefaction potential (L_p), as shown in Table 2. I_B, CP, and L_p were calculated using Eqs. 1, 2, and 3, as mentioned in Thevanayagam et al. (2002) and (Casagrande 1975), respectively.

$$I_B = \frac{s_u(\text{yield}) - s_u(\text{liq})}{s_u(\text{yield})} \tag{1}$$

$$\text{CP} = \frac{p_i' - p_{ss}'}{p_i'} \tag{2}$$

$$L_p = \frac{\sigma_{3i}' - \sigma_{3f}'}{\sigma_{3f}'} \tag{3}$$

where $s_u(\text{yield}) = q_{max}$; $s_u(\text{liq}) = q_{min}$; p'_i = initial effective confining pressure; p'_{ss} = effective confining pressure at steady state; σ'_{3i} = initial minor principal stress; and σ'_{3f} = minor principal stress at the end of shearing.

The liquefaction indices for SU3 were highest and in agreement with large Δu and subsequent loss in shear strength, resulting in static liquefaction in soil site 3. The I_B value was the same for SU1 and SU2 as the ratio of difference of peak deviatoric stress and steady-state strength to the peak deviatoric strength was the same for both the soil samples. The value of CP was obtained to be higher for SU1 as compared to SU2. Liquefaction potential was evaluated and analyzed based on the global void ratio (e), intergranular void ratio (e_s), and interfine void ratio (e_f). The intergranular and interfine void ratios were computed using Eqs. 4 and 5, as proposed by Thevanayagam (1998).

$$e_s = \frac{e + \text{FC}/100}{1 - \text{FC}/100} \tag{4}$$

$$e_f = \frac{e}{FC/100} \tag{5}$$

The variation in L_p with respect to e, e_s, and e_f is shown in Fig. 3. The variation of L_p with e was found not to be prominent. The relationships between L_p with e_s and e_f were obtained to be opposite and could be attributed to the way e_s and e_f were defined. Liquefaction potential was observed to increase with the increase in e_f. At a given e, an increase in e_f represented a reduction in the sand-to-sand contacts in the fines-dominated sand-fines soil matrix. However, in the present study, both e and e_f increased simultaneously causing higher compressibility and liquefaction susceptibility. The undrained response of the loose sand-silt mixture was observed to be highly contractive leading to higher liquefaction potential. The liquefaction indices reflected that the soils from sites 1 and 3 were least and most susceptible to static liquefaction, respectively. The higher liquefaction resistance of soil from site 1 could be due to significant clay-sized particles, which possibly coated the sand and silt particles, causing a more stable and relatively dilatant microstructure. The liquefaction indices indicated that the soils from sites 1, 2, and 3 were more prone to static liquefaction under undrained conditions. The static liquefaction characteristics of cohesionless soils were also evaluated based on the state parameter (ψ), proposed by Park et al. (2000). The state parameter was defined as the difference in void ratio at the initial soil state and the steady-state conditions at given p'. The combination of initial stress state and material state would result in a unique soil state characterized through ψ. The normalized peak deviatoric stress (σ_{dmax}/σ_c) and pore pressure parameter at

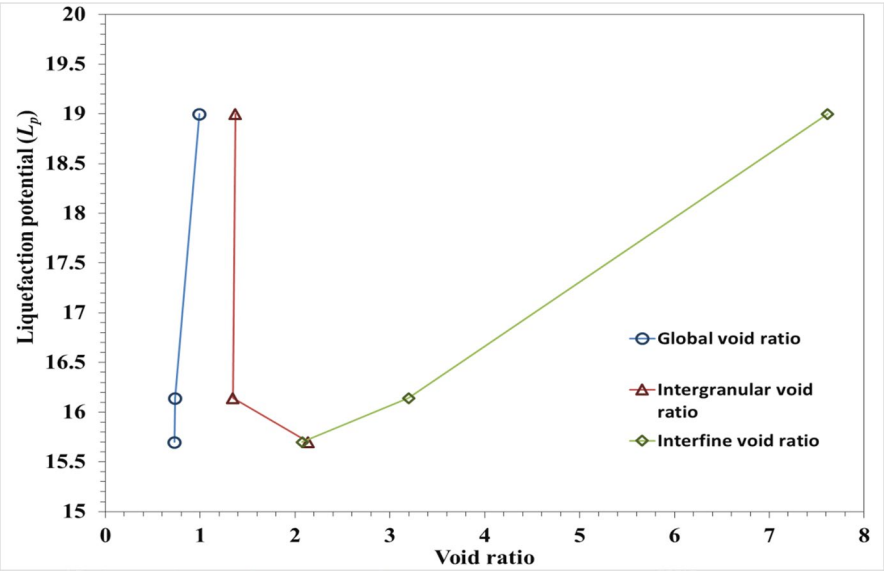

Fig. 3 Variation of liquefaction potential of soils from sites 1, 2, and 3 with respect to global, intergranular, and interfine void ratio

failure (A_f) of SU1, SU2, and SU3 are shown in Fig. 4. The soils in the present study depicted a similar but slightly scattered response, as shown by Kogyuk soils (Rahman and Lo 2014). The soils in the present study displayed slightly higher normalized peak deviatoric stress because of the presence of FC > 10%. Although

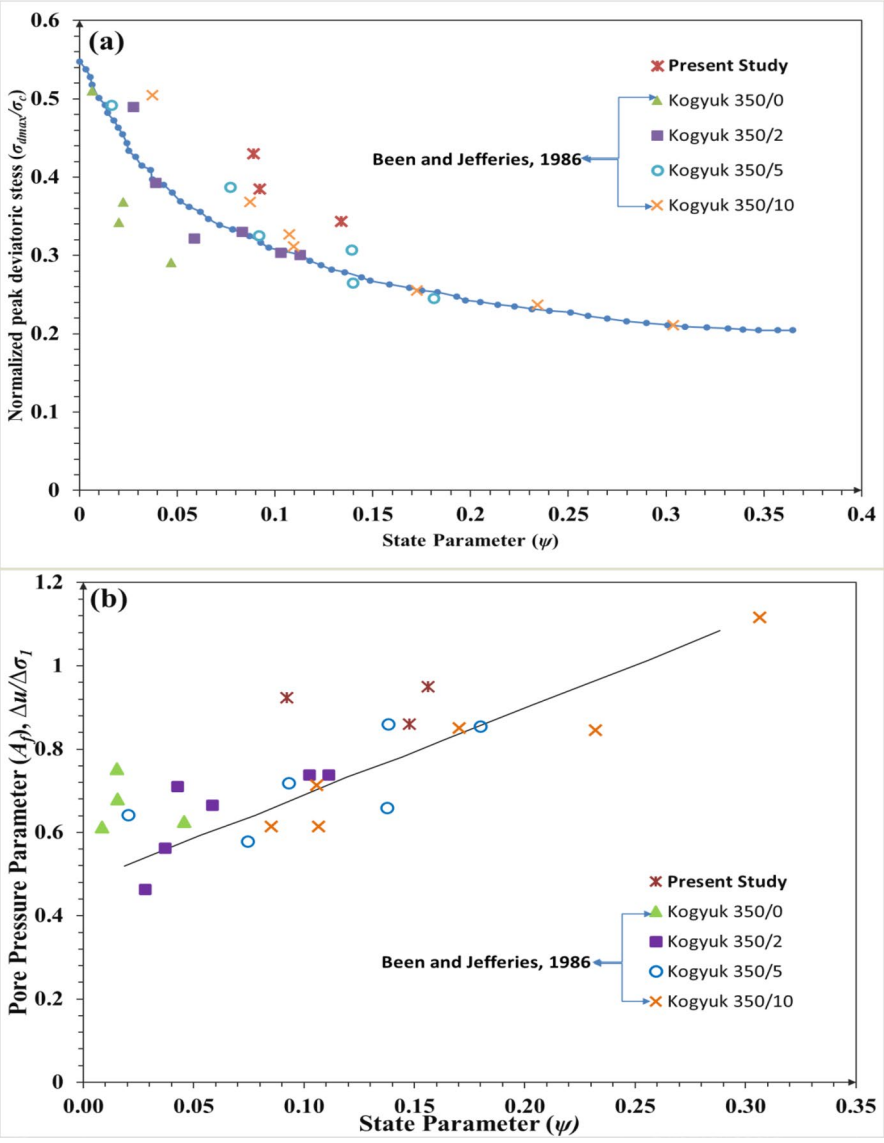

Fig. 4 Comparison of the present study with previous studies conducted by Been and Jefferies (1986). **a** Peak undrained shear strength as a function of state parameter. **b** Pore pressure at failure as a function of state parameter

the two studies were based on different soils, there was an overall good correlation between the state parameter and normalized deviatoric stress. The A_f value greater than or close to 0.9 indicated a large Δu and low deviatoric stress indicating high liquefaction susceptibility. Irrespective of the FC, the material state of the soil governed the undrained soil behavior (Fig. 4b).

3.2 Liquefaction Susceptibility Under Different Stress States

Instability in soil mass is a function of the current stress and material states under imposed undrained loading. The line joining the peak of the effective stress path and the stress origin, instability line (IL), divides the stress space into two regions, namely stable zone and potential zone of instability (Lade 1992). To investigate the instability under completely undrained conditions, IL was plotted from the undrained compression tests SU1, SU2, and SU3, as shown in Fig. 5a, and ESR corresponding to the IL was referred to as η_{IS}. The three soils exhibited different η_{IS}, as shown in Fig. 5b. The value of η_{IS} for SU1 was higher as compared to SU2 and SU3 and could be due to the difference in the initial void ratio of the soil specimens. Instability line being a function of the material state is unique for the specimens with the same void ratio (Yang 2002). The strain softening was triggered within the specimens when the ESR became equal to η_{IS}. DFE representing the maximum ESR that could be obtained under completely drained conditions is presented in Fig. 5a for soils from sites 1, 2, and 3. The region bounded by the IL and DFE was referred to as the zone of potential instability (Lade 2002). The effect of ESR on the instability and subsequent liquefaction was studied by applying predefined stress paths and stress states at boundary conditions that varied from completely drained to completely undrained. Four ESRs were selected for each soil to understand the effect of stress states and drainage conditions (Table 3). Figure 6a illustrates the stress states of these ESRs relative to IL and DFE. The stress–strain response for soils from sites 1, 2, and 3 are presented in Fig. 6. The specimens were tagged as Sij, where i represents the site number of the soil and j represents the ESR value. For example, S12 represented the specimen from site 1 and soil subjected to ESR2 at the start of undrained shearing. The specimens SM11 to SM14 were subjected to undrained shearing after attaining different ESRs during shearing (Fig. 6a). SM11 and SM12 were loaded in drained fashion up to very low ε_a less than 1% and achieved peak deviatoric stress (σ_{dmax}) after the imposition of undrained conditions and continued to mobilize shear stress until η_{IS} corresponding IL was achieved. SM11 and SM12 displayed stability under imposed undrained conditions, and therefore, the stress space below the IL could be referred to as a stable region. The two specimens achieved σ_{dmax} of magnitude 38 kPa and 50 kPa at strains of 1% and 1.2% respectively, and thereafter, intense post-peak softening initiated as shown in Fig. 6a. SM11 and SM12 mobilized very low steady-state shear strengths at higher ε_a signifying no further particle rearrangement with continued shearing. Similar behavior was observed in SM21, SM22, SM31, and SM32. Specimens SM21 and SM22 mobilized lower σ_{dmax} as compared to that of SM11 and SM12 owing to the different initial dry densities. In specimens SM31 and SM32, the shear strength was lost completely within 5–6%

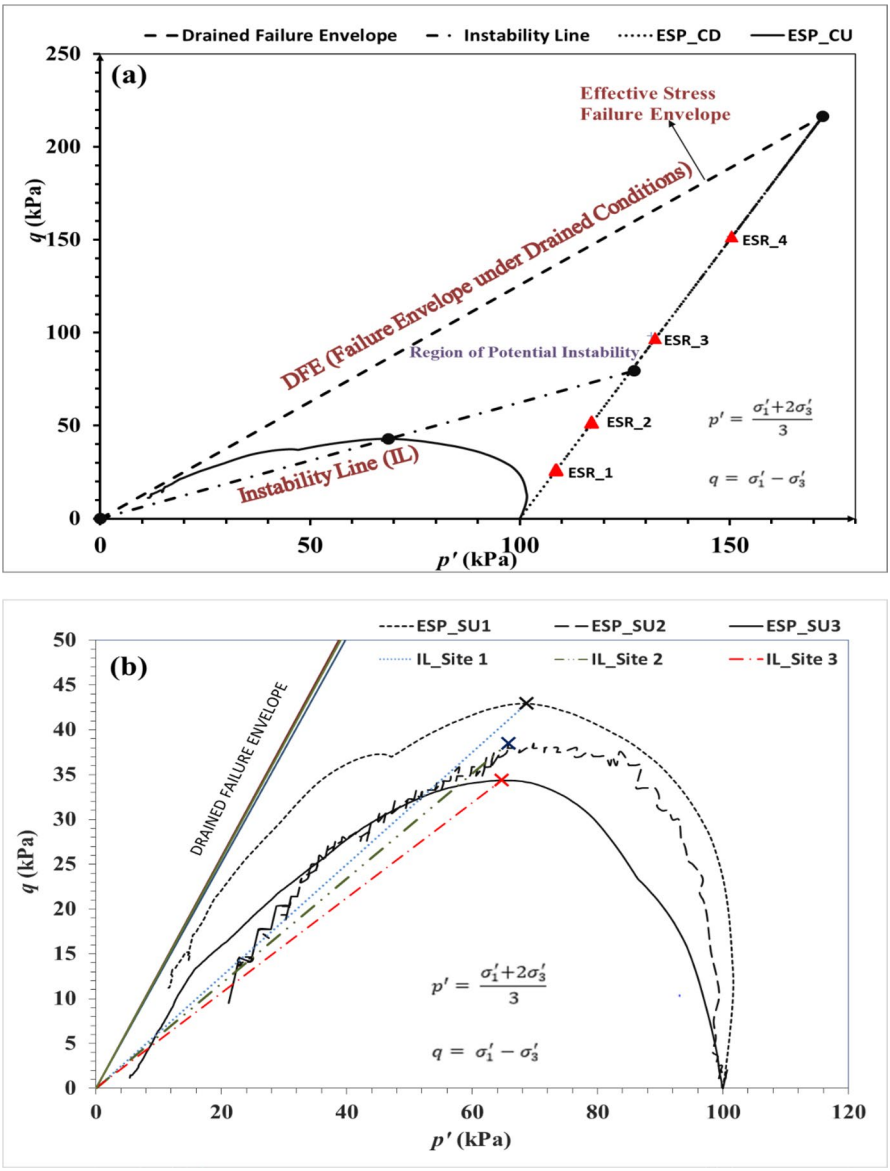

Fig. 5 Instability line and drained failure envelope of soils from sites 1, 2, and 3. **a** Experimental methodology for shearing at different ESRs. **b** Representation of IL and DFE of soils from sites 1, 2, and 3 in q-p' space

axial strains with σ_{dmax} achieved within ε_a of 2.5–3%. The complete loss of shear strength under undrained shearing was attributed to the very low initial dry density and presence of non-plastic fines. The finer silt particles sit at the contacts of the load-bearing sand grains resulting in a highly compressible metastable soil structure

Table 3 Effect of ESR on liquefaction resistance of soils from sites 1, 2, and 3

Specimen	Soil	ESR (q/p')	Strain at the imposition of undrained conditions, ε_p (%)	Peak deviatoric stress, σ_{dmax} (kPa)	Deviatoric stress at the imposition of undrained conditions, σ_{dp} (kPa)	Void ratio at the imposition of undrained conditions, e_p
SM11	Site 1	0.24	0.53	38.1	23.8	0.68
SM12		0.43	0.82	49.8	42.2	0.67
SM13		0.70	4.02	80.6	80.6	0.60
SM14		0.99	6.39	135.6	135.6	0.59
SM21	Site 2	0.24	0.37	36.0	25.4	0.67
SM22		0.45	0.71	57.1	49.6	0.66
SM23		0.629	2.04	80.3	80.3	0.58
SM24		0.89	4.67	124.3	124.3	0.57
SM31	Site 3	0.24	0.37	36.4	25.9	0.95
SM32		0.34	0.68	46.4	38.4	0.94
SM33		0.66	1.92	82.9	82.9	0.92
SM34		0.79	3.33	104.9	104.9	0.90

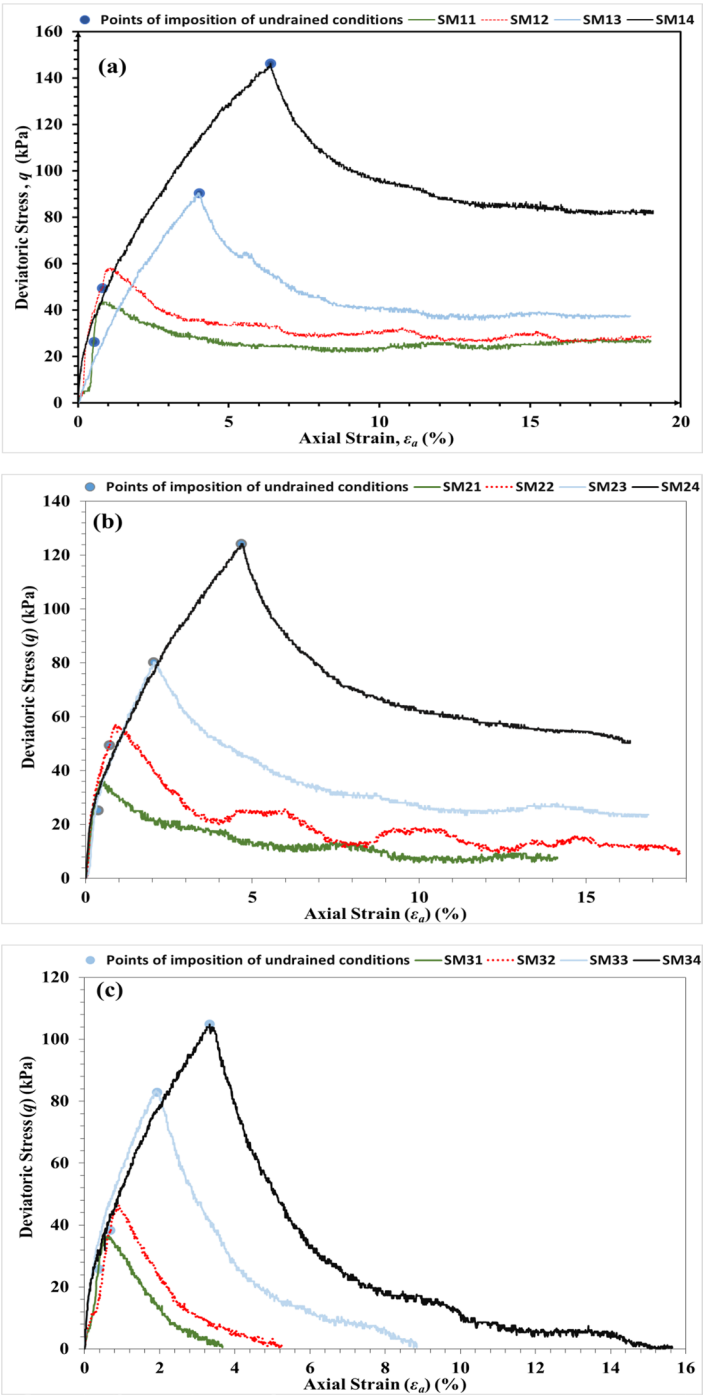

Fig. 6 Stress–strain behavior of soils from sites 1, 2, and 3 at different ESRs. **a** Response of site 1 soil. **b** Response of site 2 soil. **c** Response of site 3 soil

(Hussain and Sachan 2019c). High compressibility and low load-bearing capacity of the soil structure led to high liquefaction susceptibility. Higher ESR values, lying between IL and DFE of SU1, were imposed on SM13 and SM14 compared to SM11 and SM12. To achieve the high ESRs for SM13 and SM14, the drained shearing was conducted up to larger ε_a resulting in mobilization of higher peak deviatoric stresses compared to SM11 and SM12. As soon as the undrained conditions were imposed, a sudden drop in the deviatoric stresses was observed signifying the inability of the specimens to withstand the existing stress state under the imposed undrained conditions. Perturbance, in the form of effective stress, was responsible for the instability. The onset of strain softening was coincident with the initiation of instability within SM13 and SM14 (Md Mizanur and Lo 2012). Though the ESR for SM13 and SM14 were different, both showed a drop in deviatoric stress values as soon as the undrained conditions were imposed. If the drained shearing was continued, no instability would have been observed. Therefore, it could be concluded that the specimens exhibited unconditional instability as soon as the undrained conditions were imposed at the stress states located between IL and DFE. The instability triggered the instantaneous generation of large Δu leading to an abrupt reduction in deviatoric stress. Specimens SM23, SM24, SM33, and SM34 displayed similar behavior, as shown in Fig. 6b, c. Deviatoric stress mobilized by the specimens varied with ESR, as revealed from the stress–strain response of soils 1, 2, and 3. The difference in σ_{dmax} was due to the varying changes in void ratio during the drained shearing resulting in significantly different material states at the imposition of undrained conditions. Specimen with higher ESR had a lower void ratio leading to a more compact interparticle soil arrangement and causing the mobilization of higher shear strength. Significant residual strength was observed at higher ESRs due to the lower void ratio at which undrained conditions were imposed. The specimens from soil site 3 experienced complete loss in shear strength when the undrained conditions were imposed at ESRs corresponding to the region between IL and DFE. Even though large volumetric strains were induced during the drained shearing, the void ratio at the imposition of undrained conditions was still substantially higher (0.9). It signified inherently loose configuration resulting in total loss of shear strength under imposed undrained shearing. The comparison of three soils revealed that irrespective of the initial material state and composition, the soil exhibited instability when stress states at the imposition of undrained conditions were lying in the zone of potential instability. The volumetric response of soils 1, 2, and 3 at different ESRs is shown in Fig. 7. The initially loose specimens exhibited higher contractive behavior to achieve a more stable and compact particle arrangement. The magnitude of induced volumetric strains was observed to increase with the increase in ESR for all three soils. Prolonged drained shearing required to attain higher ESR resulted in a lower void ratio at the instant of the imposition of undrained conditions (Table 3). The volumetric strain for soil 1 was observed to be lower as compared to soils 2 and 3, and the difference was more prominent at higher ESR. At the imposition of undrained conditions, the volumetric strains for SM14 and SM34 were observed to be 10.5% and 5.8% for ESR values of 0.99 and 0.79, respectively. Drained shearing up to ε_a of 6.4% and 3.3% was required to attain ESR of 0.99 in SM14 and 0.79 in SM34, respectively (Fig. 7a, c). The volumetric strain in SM14 was found to be

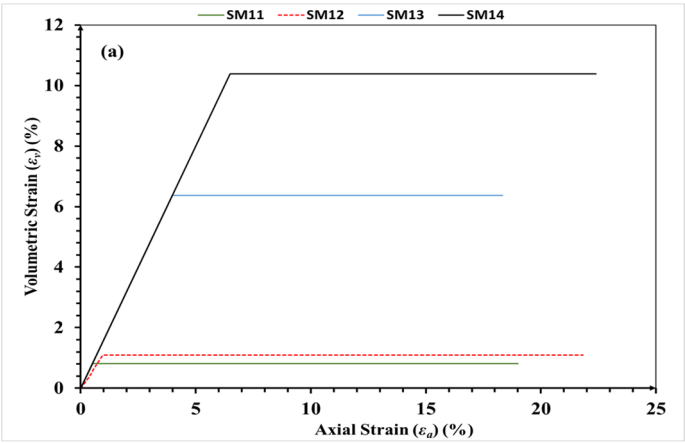

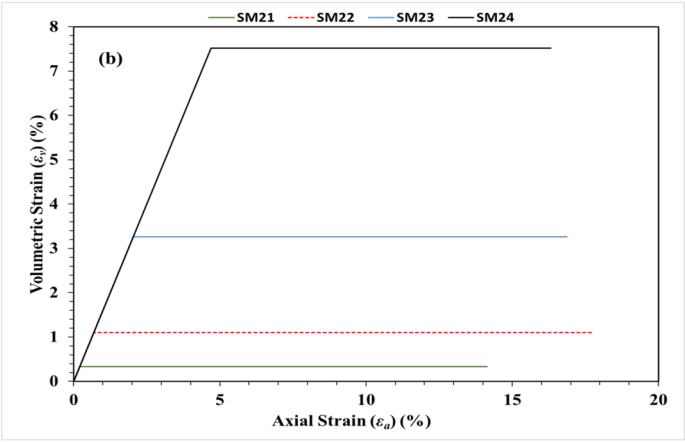

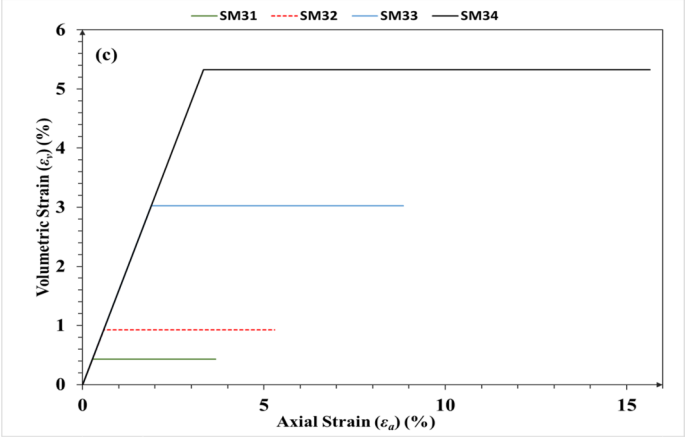

Fig. 7 Volumetric behavior of soils with the effect of radial strain from sites 1, 2, and 3 at different ESRs. **a** Response of site 1 soil. **b** Response of site 2 soil. **c** Response of site 3 soil

higher due to higher ESR and higher FC. Drained shearing up to ε_a of 6.4% to attain ESR of 0.99 resulted into large volumetric strains in SM14.

The increase in deviatoric stress was responsible for the ascending response of ESP, whereas the evolution of Δu caused a loss in p' (Fig. 8). The ESPs of SM11 and SM12 progressed towards the stress origin as soon as the undrained conditions were imposed. The rising slope of ESP indicated stable behavior for SM11 and SM12 under undrained conditions (Fig. 8a). The ESPs ascended until they intersected the IL, and further, a gradual drop in the ESP pointing towards the origin was observed. Due to the continued generation of Δu, p' decreased continuously, resulting in the reduction of shear strength. As Δu was building up, the effective contact stress between the soil particles decreased, leading to lower shear strength. Large Δu and lower shear strength signified static liquefaction within soil specimens. A similar response was observed in SM21, SM22, SM31, and SM32 (Figs. 8b and 7c). SM11 and SM12 attained steady state under undrained conditions with significant residual strength. However, ESPs of SM21, SM22, SM31, and SM32 reached nearly to stress origin, indicating a complete loss of shear strength under undrained conditions. The rate of evolution of Δu in the case of soil from site 3 was found to be higher as compared to soils 1 and 2. The ESPs of SM13 and SM14 depicted a sudden drop as soon as the undrained conditions were imposed. The drop in ESPs represented a reduction in σd and p' under imposed undrained conditions causing instability in soils. This instability was reported as solid–fluid instability or diffused instability ((Vaid and Eliadorani 1998; Lade 2002; Hussain et al. 2019)). The wrinkles observed on the latex membrane at the end of undrained shearing were similar to diffused deformations observed by Thevanayagam (1998). The specimens could not sustain the stress increments imposed by undrained conditions because of the already existing shear stresses developed under drained shearing. The stress increments under undrained shearing generated Δu initiating the onset of instability and consequently leading to static liquefaction. A similar response was also observed for SM23, SM24, SM33, and SM34, even though the stress states and material states differed for all the specimens. The ESPs of soils 1, 2, and 3 under undrained shearing approached DFE and displayed asymptotic response at large strains. At the same ESR, p' at steady state was different for soils 1, 2, and 3. Soil 1 exhibited higher p' as compared to soils 2 and 3. The lowest steady-state shear strength due to lowest p' was observed for soil 3. Even though the specimens had different material states at the point of the imposition of undrained conditions, the soils exhibited instability if their stress states were located in the region of potential instability. A similar response was reported by Vaid and Eliadorani (1998) and (Daouadji et al. 2010). The results showed that the instability in silty sands under undrained conditions would be unconditional. (Vaid and Eliadorani 1998) conducted strain path testing to study the influence of partially drained conditions on the instability behavior of silty sands. The drainage during shearing was reported to play an important role in the evolution of the failure mechanism, and even minimal volumetric strains were reported to have the potential to trigger the instability at constant shear stress that would not develop under completely undrained conditions.

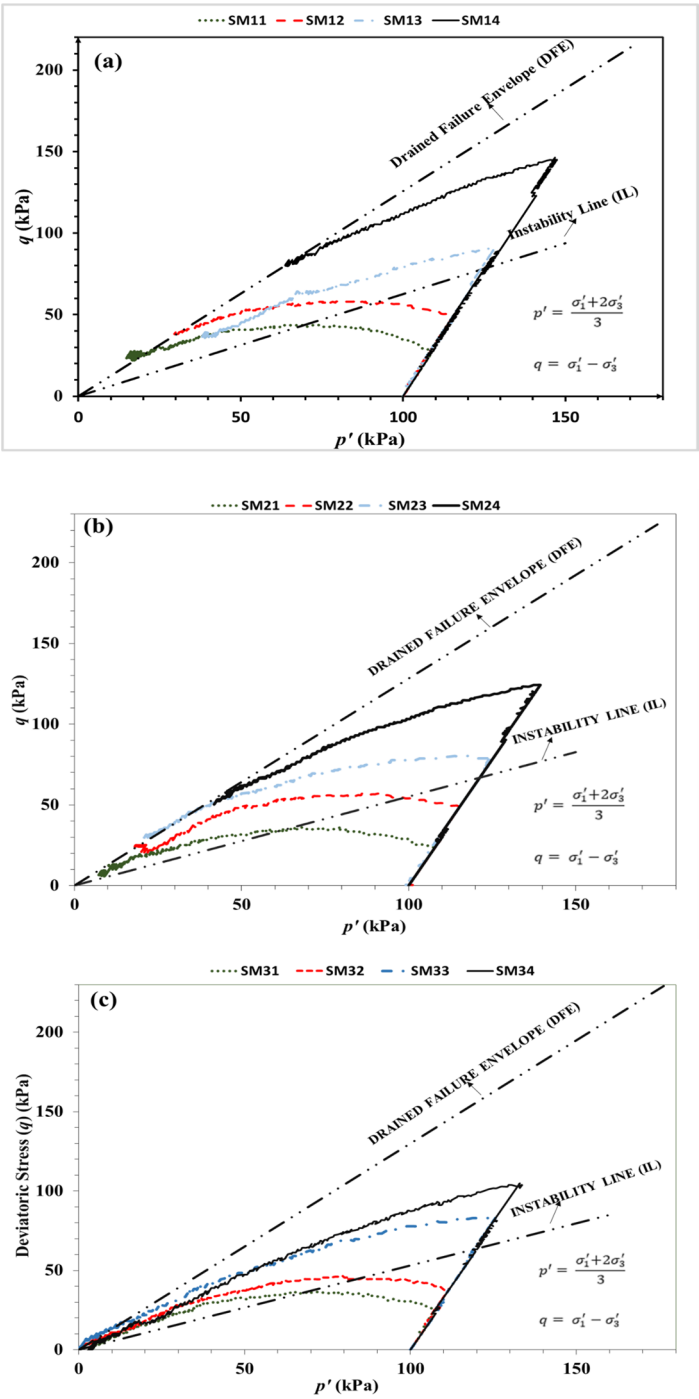

Fig. 8 Effective stress paths in q-p' space of soils from sites 1, 2, and 3 at different ESRs. **a** Response of site 1 soil. **b** Response of site 2 soil. **c** Response of site 3 soil

The volumetric strains under drained shearing were analogous to excess pore water under undrained shearing. (Chu et al. 2003) proposed a new framework to analyze the instability of slopes with granular soils. The stress states were identified, and their locations within q-p' stress space were observed to dominate the soil's behavior under undrained conditions. (Chu et al. 2003) described undrained instability as runaway instability and drained instability as conditional instability. (Chu and Leong 2002) reported instability in silty sands under mix drained shearing at constant deviatoric stress. The instability curve as the relationship between void ratio and ESR at the onset of instability was developed. The relationship was verified by conducting undrained tests at different ESRs. The ESR, at which instability was triggered, coincided with the instability curve of void ratio with ESR. The present study results were found to be in good agreement with those by the (Chu and Leong 2002).

3.3 Liquefaction Susceptibility Under Cyclic Simple Shear Conditions

The hysteresis response for the first loading cycle of soils from sites 1, 2, and 3 at different cyclic stress ratios is depicted in Fig. 9a. Specimens with lower CSR sustained cyclic loading for greater than 1000 cycles without much loss in shear strength, while specimens with higher CSR exhibited a complete loss in shear strength at a comparatively lower number of cycles. Therefore, the hysteresis loop for the first loading cycle of each test was plotted to study the effect of CSR on the cyclic simple shear behavior of soils from sites 1, 2, and 3. It was observed that the shear strain during the first cycle increased with the increase in CSR for all soils. The observed response was expected due to the increase in loading intensity, and the specimens would exhibit higher deformations. The shear strain on the compression side was found to be more as compared to the shear strain on the extension side irrespective of the CSR and the soil type. The highly asymmetrical hysteresis response of shear strain in the C33 specimen at CSR of 0.01 could be due to the high initial void ratio signifying a very loose soil matrix. The evolution of excess pore pressure during the first cycle was 10% of the applied normal pressure for specimen C33. The application of loading stresses on the specimen resulted in considerable deformation on the compression side. However, during the unloading part of the first cycle in the C33 specimen, the soil specimen recovered only a small part of the compressive strain. This could be attributed to the bias created during the first yielding of the soil specimen resulting in the accumulation of plastic strains on one side. Figure 10 displays the accumulated shear strain versus the number of loading cycles at different CSR for all soils. The accumulated shear strain was calculated using Eq. 6 given by Thian and Lee (2017). The accumulated shear strains at the end of the first and last loading cycles are shown in Table 4. The accumulated shear strains were observed to increase with an increase in the CSR for cohesionless soils (Andersen 2004; Erken and Can Ulker 2007). However, a sudden jump in the accumulated shear strain was observed at the instant of liquefaction. It was found that the accumulated shear strain in the C24 specimen increased from 0.13 to 0.28% in five loading cycles and further

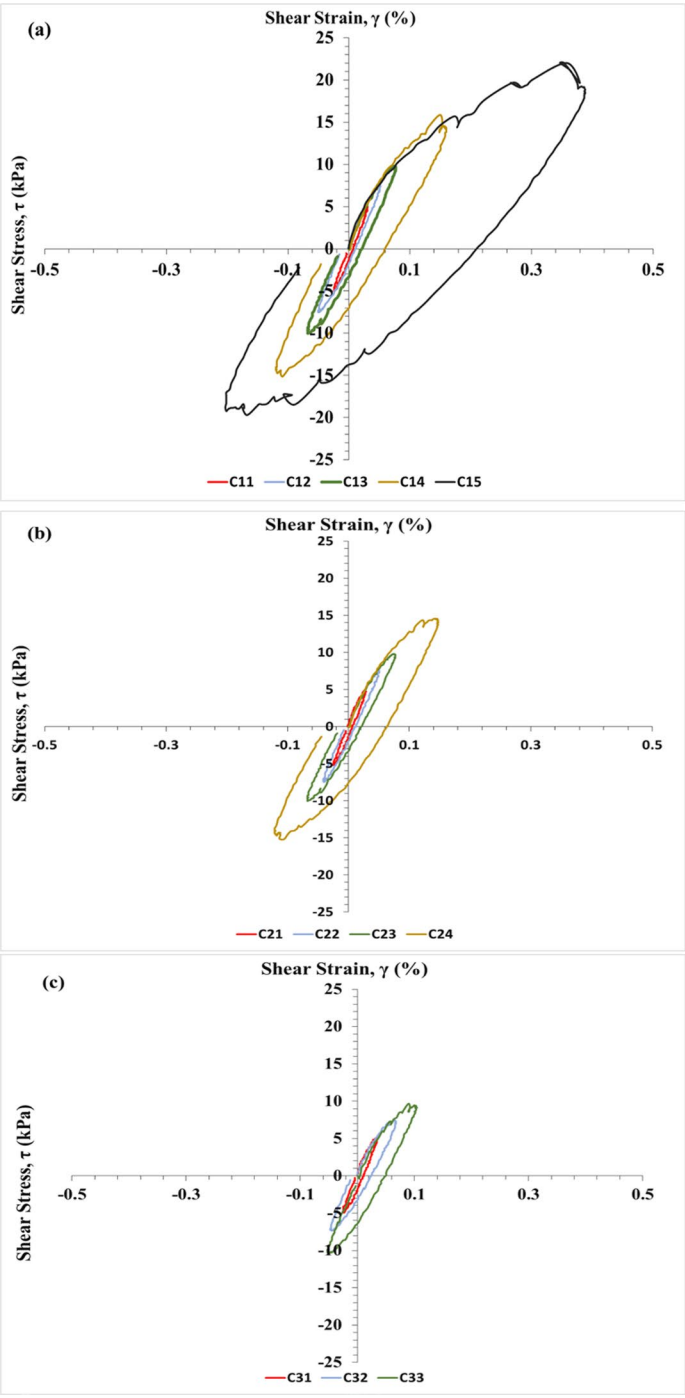

Fig. 9 Effect of CSR on the hysteresis response of soils from sites 1, 2, and 3 under CSS loading conditions. **a** Site 1. **b** Site 2. **c** Site 3

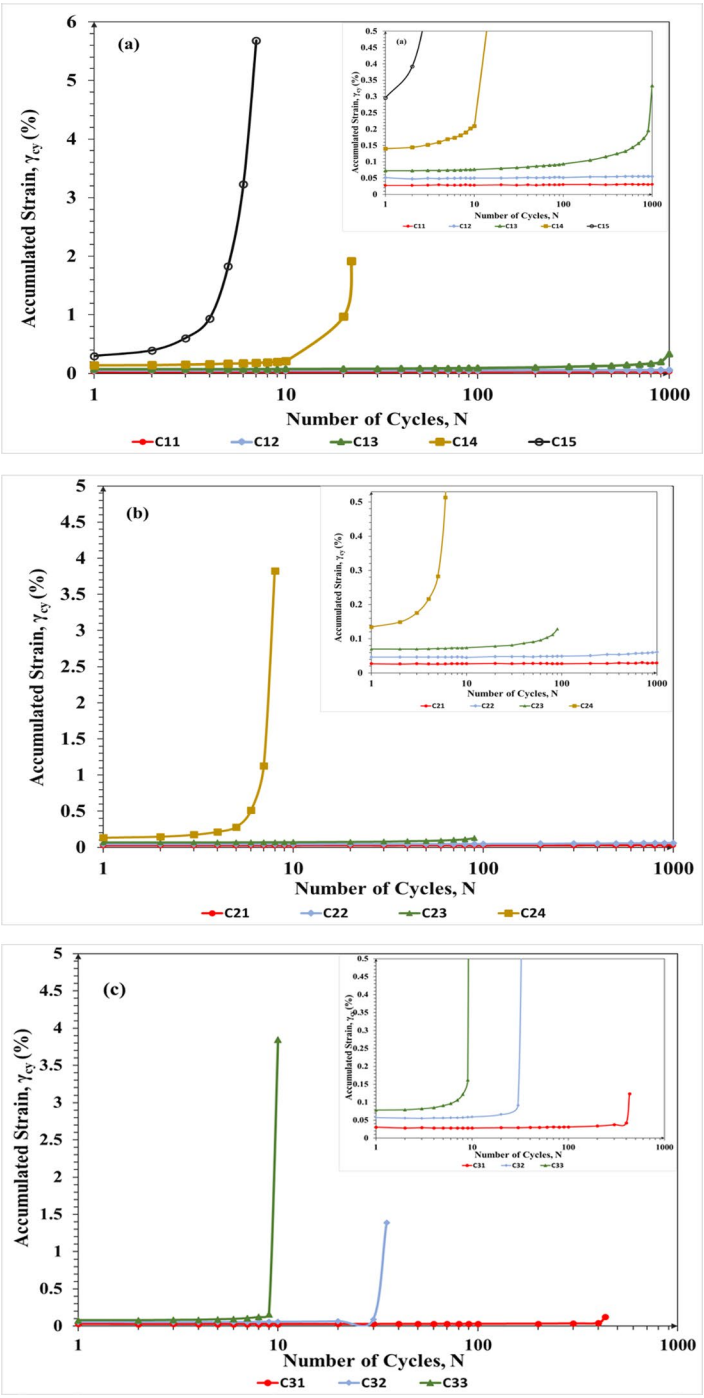

Fig. 10 Effect of CSR on the accumulated shear strain response of soils from sites 1, 2, and 3 under CSS loading conditions. **a** Site 1. **b** Site 2. **c** Site 3

increased 3.8% by the 8th cycle. The sudden increase in the rate of accumulation of shear strain within the soil mass could be due to the initiation of cyclic liquefaction within the soil mass, leading to large shear deformations. Similar findings for sands were reported under stress-controlled cyclic triaxial tests (Eskisar et al. 2014). The sudden jump in the accumulated shear strain values reflected the major loss of shear strength. The specimens exhibited flow-like behavior, which was reflected through these large and uncontrolled shear strains. The number of cycles required for liquefaction decreased with the increase in CSR (Table 4). The soil structure experiences severe degradation due to the application of a higher load. Large intensity loading also contributes to the accumulation of higher excess pore water pressure resulting in liquefaction in fewer cycles (Thian and Lee 2017). The excess pore pressure response at different CSR is shown in Fig. 11. The evolution of excess pore water pressure was represented through the excess pore pressure ratio (r_u), which was defined as the ratio of excess pore water pressure (Δu) and initial vertical overburden pressure (σ_{vi}). In the present study, the evolution of r_u equal to 0.9 or more was considered as the criteria for liquefaction. The strain amplitude (SA) criterion as per the ASTM code (ASTM D5311, D5311M 2013) was also applied for all CSS test results. The number of cycles required to induce SA of 3.75% was determined. The number of cycles was always found to be higher for the SA criterion than the pore pressure ratio criterion ($r_u > 0.9$). Thus, in the present study, pore pressure ratio criterion was chosen to represent the more critical case for liquefaction analysis. It was observed that the excess pore water pressure increased with the increase in the number of loading cycles. The specimens C13, C14, and C15 displayed r_u greater than 0.9 indicating the initiation of liquefaction within the soil mass in 1000, 22, and 10 cycles respectively. It was also noted that at the same CSR, C22 exhibited liquefaction, but C12 did not liquefy even up to 1000 cycles. Similarly, C22 was found to liquefy in 1000 cycles, whereas C32 liquefied in 35 cycles (Table 4). Soil behavior shown in Figs. 10 and 11 was found to be aligning properly with respect to pore pressure and strain accumulation. As the excess pore water pressure increased (Fig. 11), the effective confinement decreased leading to the reduction in strength, which resulted into a large and rapid accumulation of cyclic shear strains (Fig. 10). Although the CSR was the same for all soil specimens, the different initial material states (void ratio and fines content) of the specimen led to varying liquefaction resistance.

$$\gamma_{cy} = \frac{\gamma_{max} - \gamma_{min}}{2} \tag{6}$$

Dynamic properties were evaluated from the hysteresis loops at different cycles up to 1000 loading cycles. Shear modulus (G) and damping ratio (D) were evaluated using Eqs. 7 and 8, respectively, as described by Kramer (1996). The relationship between shear modulus and accumulated strain is shown in Fig. 12. The shear modulus was observed to decrease with an increase in accumulated strain for all CSRs (Fig. 12a). The soils from sites 2 and 3 also displayed a similar response. During undrained cyclic loading, generation of high excess pore water pressure causes loss of intergranular forces resulting in reduced effective stress and soil stiffness.

Table 4 Liquefaction resistance of cohesionless soils at different CSR under CSS loading conditions

				Parameters at the end of first cycle			Parameters at the end of last cycle			
Soil type	FC	Specimen	CSR	Accumulated strain (γ_{cy}), %	r_u	G_0, Mpa	Accumulated strain (γ_{cy}), %	r_u	G, Mpa	N_L
Site 1	45	C11	0.05	0.027	0.011	18.39	0.031	0.24	16.44	> 1000
		C12	0.075	0.051	0.022	14.63	0.055	0.4	13.62	> 1000
		C13	0.1	0.072	0.039	13.67	0.33	0.94	2.89	1000
		C14	0.15	0.096	0.085	10.25	0.115	0.98	9.35	22
		C15	0.2	0.29	0.21	6.36	20.37	0.97	0.074	10
Site 2	26	C21	0.05	0.026	0.03	18.56	0.029	0.4	16.44	> 1000
		C22	0.075	0.046	0.039	16.31	0.061	0.94	12.41	1000
		C23	0.1	0.07	0.039	14.11	7.08	0.97	0.52	97
		C24	0.15	0.13	0.15	10.69	14.7	0.99	0.09	9
Site 3	16	C31	0.05	0.031	0.035	16.11	0.12	0.78	11.39	433
		C32	0.075	0.058	0.066	12.66	3.46	0.98	1.94	35
		C33	0.1	0.079	0.111	12.34	20.67	1.01	0.22	10

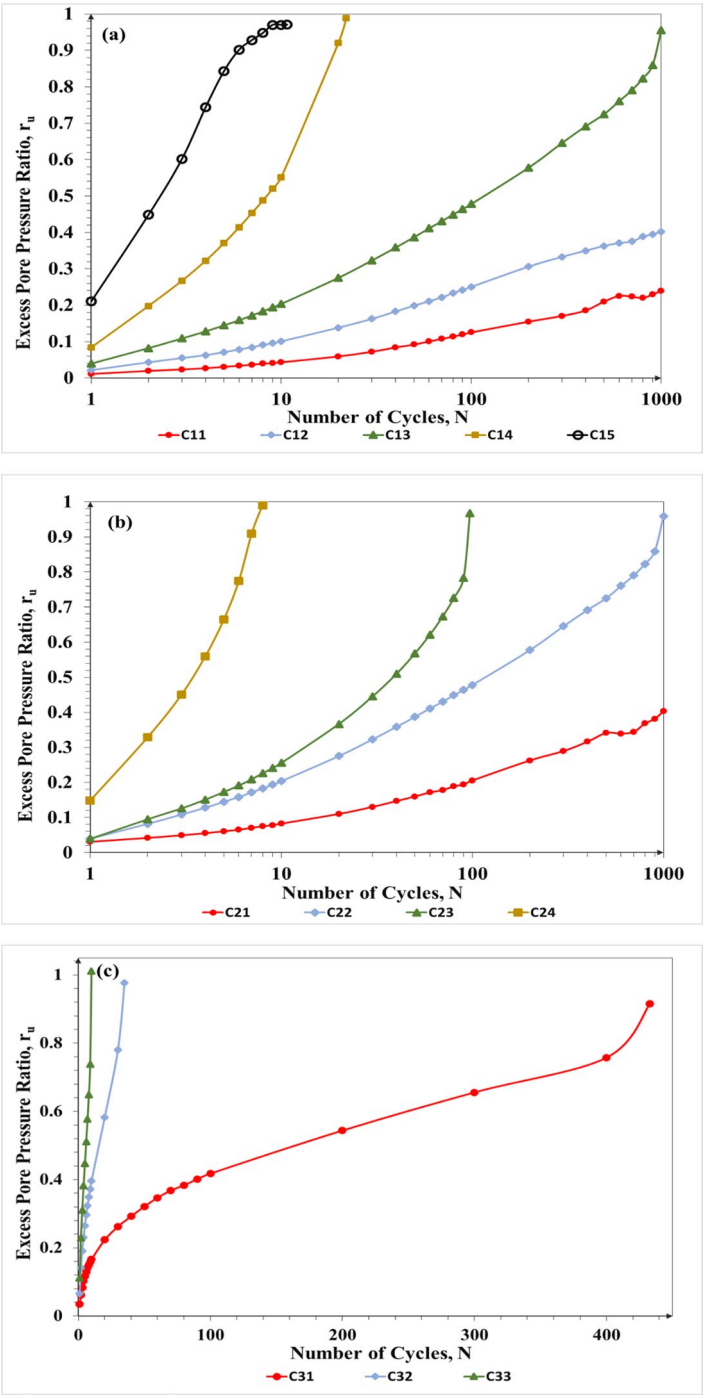

Fig. 11 Effect of CSR on excess pore pressure response of soils from sites 1, 2, and 3 under CSS loading conditions. **a** Site 1. **b** Site 2. **c** Site 3

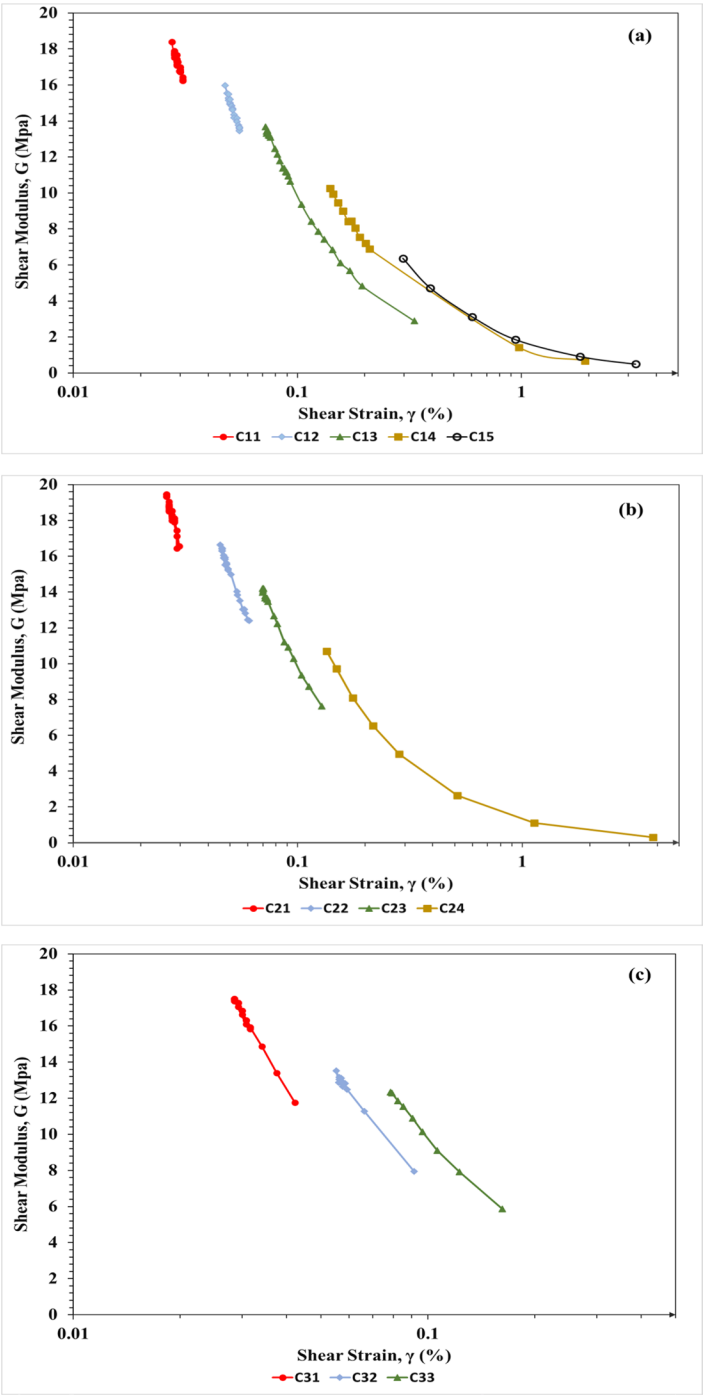

Fig. 12 Effect of CSR on shear modulus of soils from sites 1, 2, and 3 at different accumulated shear strains under CSS loading conditions. **a** Site 1. **b** Site 2. **c** Site 3

Reduction in stiffness and strength was confirmed through the accumulation of shear strains resulting in a decrease in shear modulus. During the first loading cycle, the shear modulus (G_0) was found to be nearly the same for soils from sites 1 and 2, whereas the G_0 values for soil from site 3 were observed to be the lowest at the given CSR (Table 4). The shear modulus during the last cycle was observed to be nearly zero at high CSR for cohesionless soils. The excess pore water pressure reached attained values nearly equal to the applied vertical stress indicating cyclic liquefaction. The relationship between the damping ratio and accumulated strain is shown in Fig. 13. The damping ratio was observed to increase with an increase in accumulated shear strain at all CSRs. It was observed that an increase in the damping ratio was significant at higher CSR. The variation of damping ratio with the number of cycles for all three soils is shown in Fig. 14. The damping ratio was observed to change insignificantly with the increase in the number of loading cycles until the initiation of liquefaction. In the stress-controlled cyclic simple shear testing, the shape of the hysteresis loop was observed to depend on the accumulated shear strains within the soil mass. Before the initiation of cyclic liquefaction, the change in shear strains with the number of loading cycles was observed to be insignificant, which led to almost the same area under the hysteresis loop. This could be the underlying reason for the insignificant change in the damping ratio with the number of cycles until the state of liquefaction was attained. However, at the instant of cyclic liquefaction, a sudden jump in the damping ratio was reported at all CSR. (Dash and Sitharam 2016) reported a similar damping ratio response of poorly graded sand under cyclic triaxial conditions. This was attributed to the loss of control in the load application because, as the specimen liquefied, high energy dissipation occurred. Therefore, a high damping ratio at the instant of cyclic liquefaction was observed. The variation in damping ratio was found to be evident with respect to the accumulated shear strains; however, the variation was insignificant with the number of loading cycles.

$$G = \frac{\tau_{\max} + \tau_{\min}}{\gamma_1 + \gamma_2} \tag{7}$$

$$D(\%) = \frac{\mathrm{Areaofhysteresisloop}(A_{\mathrm{L}})}{4\Pi A_{\Delta}} \times 100 \tag{8}$$

The effect of initial material state and CSR on the cyclic degradation index (δ) is shown in Fig. 15. The cyclic degradation index at various loading cycles is evaluated using Eq. 9 as mentioned in Kramer (1996) and (Boulanger et al. 1998) and is shown in Table 4. It was observed that the stiffness of the specimen reduced with the number of cycles and could be attributed to the reduced effective stresses resulting in increasing accumulated shear strain. However, the specimens subjected to higher CSR exhibited a rapid decrease in the cyclic degradation index as compared to the specimens subjected to lower CSR (Fig. 15). The higher loading intensity resulted in the rapid loss of interparticle bonds, causing a decrease in effective stress and soil stiffness. The lower or zero value of stiffness degradation indicated the loss strength within the soil mass, signifying cyclic liquefaction (Fig. 15a).

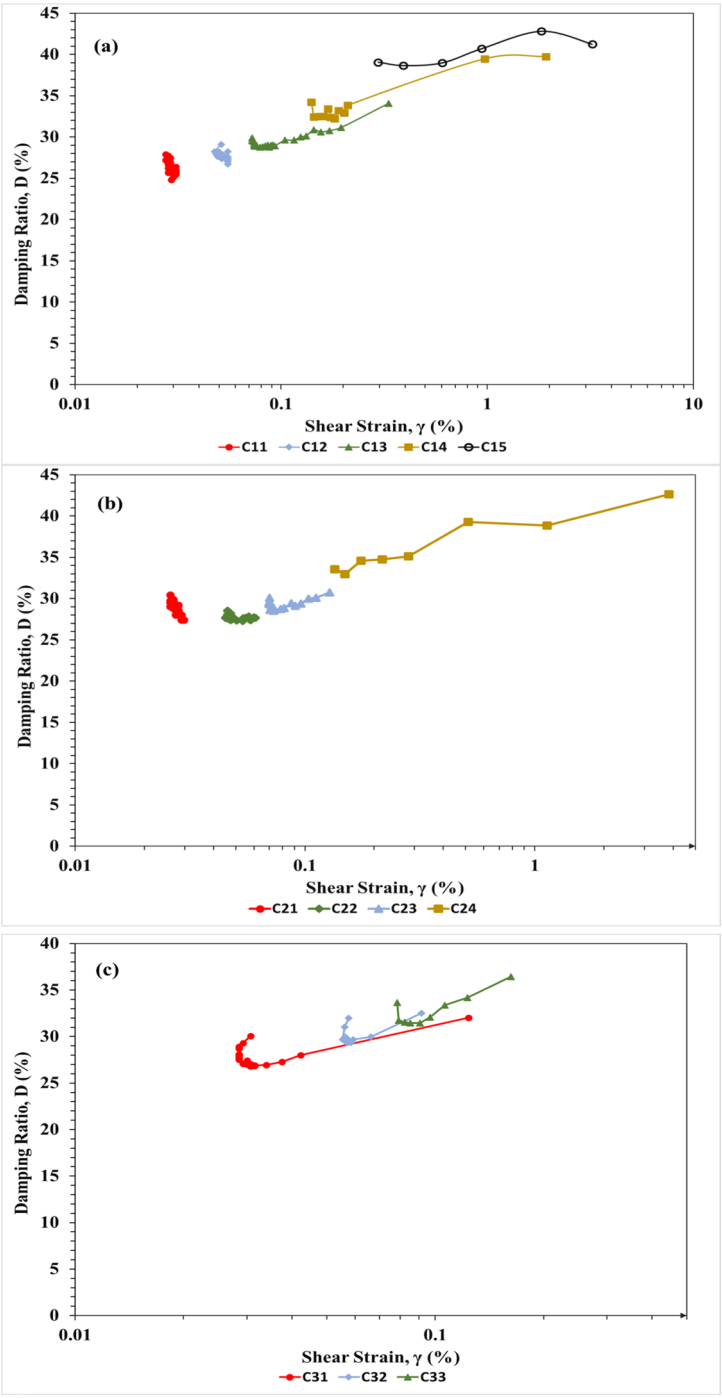

Fig. 13 Effect of CSR on damping ratio of soils from sites 1, 2, and 3 at different accumulated shear strains under CSS loading conditions. **a** Site 1. **b** Site 2. **c** Site 3

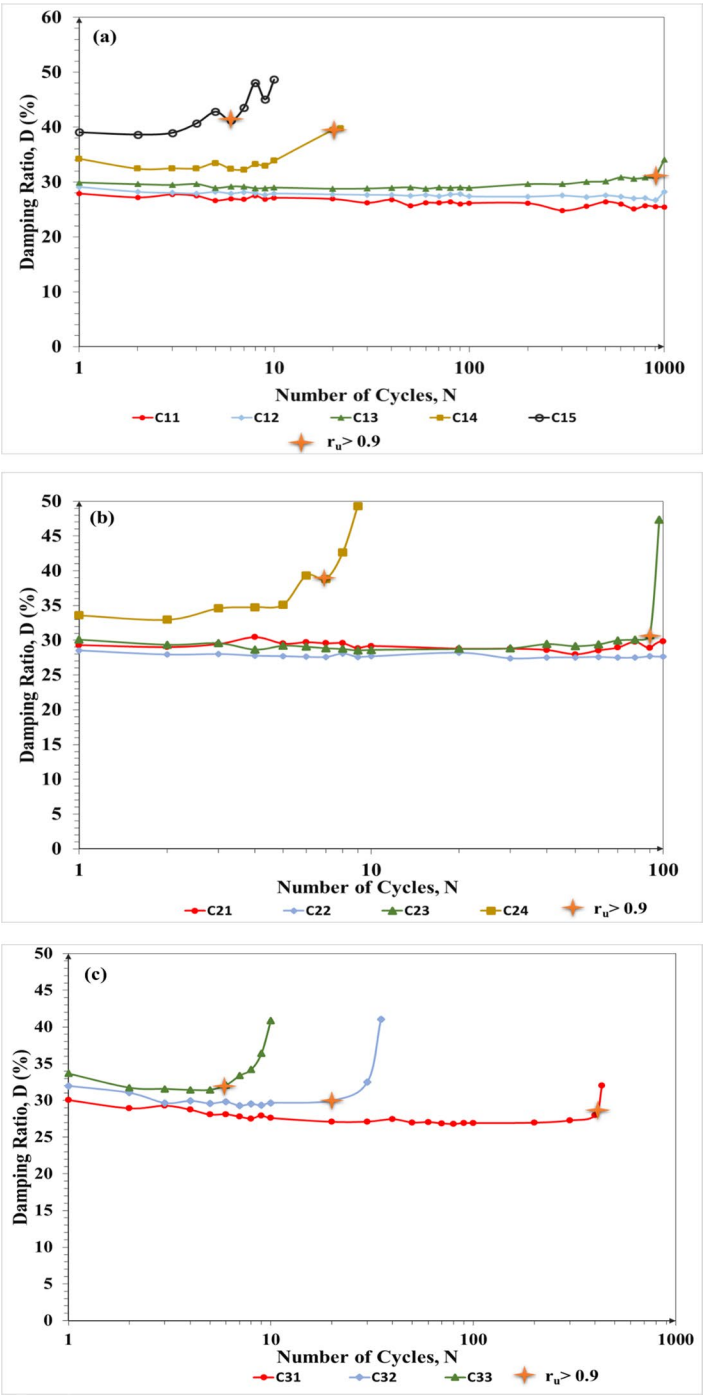

Fig. 14 Effect of CSR on damping ratio of soils from sites 1, 2, and 3 at different numbers of loading cycles under CSS loading conditions. **a** Site 1. **b** Site 2. **c** Site 3

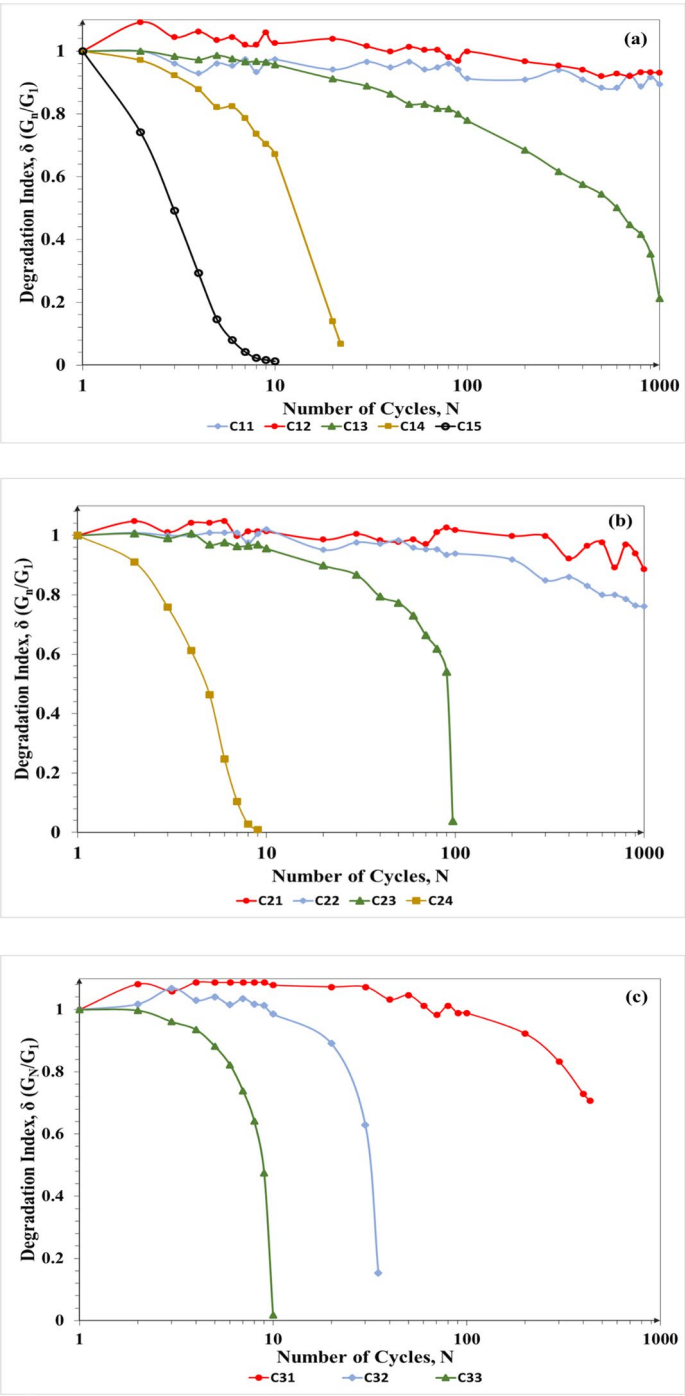

Fig. 15 Effect of CSR on degradation index of soils from sites 1, 2, and 3 under CSS loading conditions. **a** Site 1. **b** Site 2. **c** Site 3

$$\delta = \frac{G_N}{G_1} \tag{9}$$

Cyclic liquefaction resistance was evaluated for soils from three different sites in Kutch region. It was defined as the cyclic stress ratio required to initiate liquefaction in fifteen loading cycles. The criteria of fifteen loading cycles were taken as the equivalent of an earthquake of magnitude 7.5 (Ishihara 1996). Figure 16 shows the relationship of cyclic stress ratio (CSR) and the number of cycles required to initiate liquefaction (N_L) for cohesionless soils. Experimental results of specimens C11, C12, and C21 are excluded as they did not liquefy in 1000 cycles. It is evident from Fig. 16 that the cyclic resistance was observed to be highest for soil from site 1, i.e., 0.17. The cyclic resistance ratio (CRR) was determined for cohesionless soils, as shown in Table 4. The cyclic resistance was found to be dependent on the initial material state of the specimen, i.e., fines content and initial void ratio. Similar results were reported by Almani et al. (2013). The soil from site 3, with a fines content of 16% and an initial void ratio of 0.99, exhibited the lowest cyclic liquefaction resistance. The soil also exhibited the highest liquefaction potential under monotonic compression loading (Fig. 6c). It could be possible that the fines content occupied few of the void spaces and also the spaces between load-bearing sand grains. This resulted in the unstable and compressible interparticle soil arrangement in soil from site 3, leading to the collapse of the metastable structure, responsible for the highest liquefaction potential of soil.

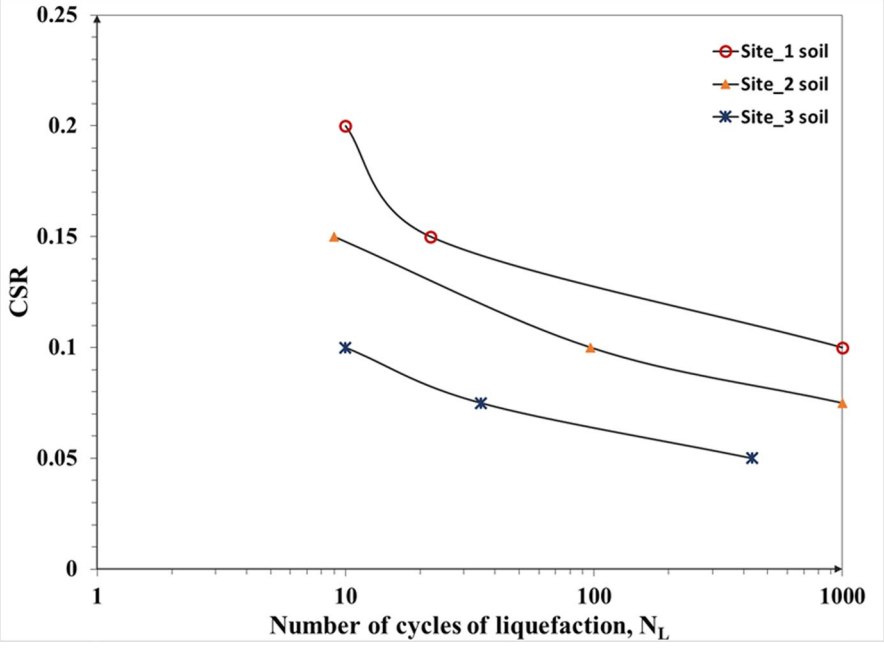

Fig. 16 Cyclic resistance of soils from sites 1, 2, and 3 under CSS loading conditions

4 Conclusions

In the present study, the influence of stress state (ESR, CSR) on the liquefaction potential of three different naturally occurring silty sands (cohesionless soils) were studied under monotonic compression and cyclic simple shear (CSS) loading at different shearing modes (drained/undrained/partially drained). The effect of CSR on the liquefaction susceptibility of naturally occurring cohesionless soils was also determined in terms of CRR of soil under earthquake shaking. The key observations from the study are as follows:

1. Silty sands exhibited undrained instability as soon as the maximum ESR was achieved. The instability line (IL) represented the upper bound of stable and lower bound of unstable stress space. The slope of IL was found to depend on the initial material state of the soil sample.
2. Specimens with stress states lying in the region of stress space below IL exhibited stable behavior under imposed undrained conditions. However, with continued deformation under undrained conditions, the specimens exhibited a very high tendency for static liquefaction.
3. Specimens with stress states between IL and DFE exhibited instability under imposed undrained conditions. Minor perturbance in the form of effective stress could initiate instability if stress states would lie between IL and DFE.
4. No significant influence of initial material states and drainage boundary conditions was observed on the instability behavior of silty sands. The inherently loose soils under imposed undrained conditions exhibited the generation of large and rapid Δu leading to instability followed by static liquefaction.
5. The critical state strength increased with the increase in imposed ESR. For higher ESR, the larger volumetric strains were required to achieve stress states resulting in a lower void ratio at the imposition of undrained conditions, subsequently leading to higher critical state strength.
6. The shear modulus and degradation index were observed to decrease with the number of loading cycles and accumulated shearing strains. The damping ratio did not change much until the initiation of liquefaction. However, it was observed to show a significant increase with the increase in accumulated shear strains.
7. It was found that the CRR of soil from sites 1, 2, and 3 was 0.17, 0.14, and 0.08. Therefore, the cyclic resistance of soils was found to be dependent on the initial material state of the soil collected from the soil site.

Acknowledgements Financial support from IIT Gandhinagar is gratefully acknowledged. Any opinions, findings, and conclusions or recommendations expressed in this material are those of the authors and do not necessarily reflect the views of IIT Gandhinagar.

Author Contribution SG: She has conducted all the experiments. She has also completed data analysis of all the cyclic simple shear and advanced triaxial tests including basic soil testing.

MH: He has trained/helped SG to conduct cyclic simple shear and advanced triaxial tests including final analysis of data.

AS: She has introduced these research ideas. She has helped in writing the paper and done review and editing this research work in all the phases of paper publishing.

Funding The research is funded by IIT Gandhinagar. IIT Gandhinagar has provided access to all the research facility and purchase of consumables and contingency for this research work. Stipend of MTech (SG) and PhD (MH) students were also funded by IIT Gandhinagar. Designing the research problem, performing experiments, data analysis, and writing of the paper have been solely the responsibility of the faculty member (AS), not the Institute (IIT Gandhinagar).

Data Availability The datasets used and/or analyzed during the current study are available from the corresponding author on reasonable request.

Declarations

Ethics Approval and Consent to Participate Not applicable. This manuscript is based on experiments conducted on soil samples. This manuscript does *not* report on or involve the use of any animal or human data or tissue. This manuscript does *not* report any studies involving human participants, human data, or human tissue.

Consent for Publication Not applicable. This manuscript does not contain data from any individual person.

Competing Interests The authors declare no competing interests.

References

Almani, Z., Ansari, K., Memon, N.A.: Liquefaction potential of silty sand in simple shear. Mehran Univ Res J Eng Technol **32**(1), 85–94 (2013)

Amini, F., Qi, G.Z.: Liquefaction testing of stratified silty sands. J Geotech Geoenviron Eng **126**(3), 208–217 (2000)

Andersen KH.: Cyclic clay data for foundation design of structures subjected to wave loading. *International conference on cyclic behaviour of soils and liquefaction phenomena*. AA Balkema Publishers,Bochum, 371–387 (2004)

ASTM D4767–04 Standard test method for consolidated undrained triaxial compression test for cohesive soils. ASTM International, West Conshohocken, PA (2018)

ASTM D5311/D5311M Standard test method for load controlled cyclic triaxial strength of soil. ASTM International, West Conshohocken, PA (2013)

Belkhatir, M., Arab, A., Schanz, T., Missoum, H., Della, N.: Laboratory study on the liquefaction resistance of sand-silt mixtures: effect of grading characteristics. Granular Matter **13**(5), 599–609 (2011)

Bouferra, R., Shahrour, I.: Influence of fines on the resistance to liquefaction of a clayey sand. Proc Inst Civ Eng- Ground Improv, ICE **8**(1), 1–5 (2004)

Boulanger, R.W., Arulnathan, R., Harder, L.F., Jr., Torres, R.A., Driller, M.W.: Dynamic properties of Sherman Island peat. J Geotech Geoenviron Eng **124**(1), 12–20 (1998)

Casagrande, A.: Liquefaction and cyclic deformation of sands a critical review, p. 88. Harvard Soil Mechanics Series, Harvard University, Cambridge, Massachusetts (1975)

Chu, J., Leong, W.K.: Effect of fines on instability behaviour of loose sand. Geotechnique **52**(10), 751–755 (2002)

Chu, J., Leroueil, S., Leong, W.K.: Unstable behaviour of sand and its implication for slope instability. Can Geotech J **40**(5), 873–885 (2003)

Chu, J., Wanatowski, D.: Instability conditions of loose sand in plain strain. J Geotech Geoenviron Eng **134**(1), 136–142 (2008)

Daouadji, A., AlGali, H., Darve, F., Zeghloul, A.: Instability in granular materials: experimental evidence of diffuse mode of failure for loose sands. J Eng Mech **136**(5), 575–588 (2010)
Dash, H.K., Sitharam, T.G.: Effect of frequency of cyclic loading on liquefaction and dynamic properties of saturated sand. Int J Geotech Eng **10**(5), 487–492 (2016)
Erken, A., Can Ulker, B.M.: Effect of cyclic loading on monotonic shear strength of fine-grained soils. Eng Geol **89**(3–4), 243–257 (2007)
Erten, D., Maher, M.H.: Cyclic undrained behavior of silty sand. Soil Dynamics and Earthquake Enginnering **14**(2), 115–123 (1995)
Eskisar, T., Karakan, E., Altun, S.: Evaluation of cyclic stress–strain and liquefaction behavior of Izmir sand. Arab J Sci Eng **39**(11), 7513–7524 (2014)
Hussain, M., Sachan, A.: Dynamic characteristics of natural Kutch sandy soils. Soil Dynamics and Earthquake Engineering **125**, 105717 (2019)
Hussain, M., Sachan, A.: Dynamic behaviour of Kutch soils under cyclic triaxial and cyclic simple shear testing conditions. Int J Geotech Eng **14**(8), 902–918 (2019)
Hussain, M., Bhattacharya, D., and Sachan A.: Static liquefaction response of medium dense silty-sand of Chang Dam. *Geotechnical Special Publication*, (GSP 308), 384–394 (2019)
Hussain, M., Sachan, A.: Static liquefaction and effective stress path response of Kutch soils. Soils Found. **59**(6), 2036–2055 (2019c)
Indraratna B, Singh M, Nguyen TT, Leroueil S, Abeywickrama A, Kelly R, Neville T.: Laboratory study on subgrade fluidization under undrained cyclic triaxial loading. Can Geotech J **57**(11), 1767–1779 (2020)
Ioanna, R., Fernando, L., Arézou, M., Alexandre, F., François, V.: Liquefaction analysis and damage evaluation of embankment-type structures. Acta Geotech. **13**(5), 1041–1059 (2018)
Ishihara, K.: Soil behavior in earthquake geotechnics. Clarendon Press, Oxford (1996)
Kramer SL.: Geotechnical earthquake engineering. Prentice Hall international series, Pearson Education, Inc., and Dorling Kindersley, Inc., New Delhi, India. ISBN: 978–8131707180 (1996)
Lade, P.V.: Static instability and liquefaction of loose fine sandy slopes. J Geotech Eng **118**(1), 51–71 (1992)
Lade, P.V.: Instability, shear banding, and failure in granular materials. Int J Solids Struct **39**(13–14), 3337–3357 (2002)
Lade, P.V., Liggio, C.D.: Stability and instability of granular materials under imposed volume changes: experiments and predictions. Int J Geomech **14**(5), 04014020 (2014)
Liu, J.: Influence of fines contents on soil liquefaction resistance in cyclic triaxial test. Geotech Geol Eng **38**(5), 4735–4751 (2020)
MdMizanur, R., Lo, S.R.: Predicting the onset of static liquefaction of loose sand with fines. J Geotech Geoenviron Eng **138**(8), 1037–1041 (2012)
Monkul, M.M., Yamamuro, J.A.: Influence of silt size and content on liquefaction behavior of sands. Can. Geotech. J. **48**(6), 931–942 (2011)
Monkul, MM., Yamamuro, JA.: The effect of non plastic silt gradation on the liquefaction behavior of sand. *International Conferences on Recent Advances in Geotechnical Earthquake Engineering and Soil Dyanmics*, San Deigo, California , USA, 1–7 (2010)
Park, Y.H., Kim, S. R., Kim, S.H.., Kim, M.M.: Liquefaction of embankments on sandy soils and the optimum countermeasure against the liquefaction. 12th World Conference on Earthquake Engineering Auckland New Zealand **1170**:1–6 (2000)
Pham, H.V., Dias, D.: 3D numerical modeling of a piled embankment under cyclic loading. International Journal of Geomechanics **19**(4), 04019010 (2019)
Rahman, M.M., Lo, S.R.: Undrained behavior of sand-fines mixtures and their state parameter. J Geotech Geoenviron Eng **140**(7), 04014036 (2014)
Thevanayagam, S.: Effect of fines and confining stress on undrained shear strength of silty sands. Journal of Geotech Geoenviron Eng **124**(6), 479–491 (1998)
Thevanayagam, S., Shenthan, T., Mohan, S., Liang, J.: Undrained fragility of clean sands, silty sands, and sandy silts. J Geotech Geoenviron Eng **128**(10), 849–859 (2002)
Thian, S.Y., Lee, C.Y.: Cyclic stress-controlled tests on offshore clay. J Rock Mechanics Geotech Eng **9**(2), 376–381 (2017)
Vaid, Y.P., Eliadorani, A.: Instability and liquefaction of granular soils under undrained and partially drained states. Can Geotech J **35**(6), 1053–1062 (1998)

Wei, L.M., Yang, J.: On the role of grain shape in static liquefaction of sand–fines mixtures. Géotechnique **64**(9), 740–745 (2014)
Yamamuro, J.A., Lade, P.V.: Static liquefaction of very loose sands. Can Geotech J **34**(6), 905–917 (1997)
Yang, J.: Non-uniqueness of flow liquefaction line for loose sand. Géotechnique **52**(10), 757–760 (2002)
Zhong-Ming, H., Da, X., Ya-Xin, L., Qian-Feng, G., Han-Bing, B.: Deformation behavior of coarse-grained soil as an embankment filler under cyclic loading. Advances in Civil Engineering, Hindawi **4629105**, 1–13 (2020)